

Non-interacting spherical active particles under confinement: generalized entropy potential

Yongfeng Zhao^{1,2,*}

¹Center for Soft Condensed Matter Physics and Interdisciplinary Research & School of Physical Science and Technology, Soochow University, 215006 Suzhou, China

²School of Physics and Astronomy and Institute of Natural Sciences, Shanghai Jiao Tong University, Shanghai 200240, China

(Dated: November 12, 2021)

We study the transport of self-propelled non-interacting active Brownian particles (ABPs) and run-and-tumble particles (RTPs) in a long tube with varying width. We obtain a generalized Fick-Jacobs equation for the active particles under the condition of slow varying width and wide tubes. In the passive limit it is equivalent to particles moving in a generalized entropy potential. The entropy potential resembles its counterpart for the passive particles, with the activity not only changing the effective temperature, but also changing the effective width of the tube. The generalized entropy potential enables estimations of 1D steady-state density along the tube and the mean-escaping time out of a spindle chamber.

The transport of active particles along a long tube plays an important role in many phenomenon in both biology and physics, especially if the shape of the tube is irregular and of changing width [1, 2]. For instance, asymmetric channels are known to create ratchet flow of active particles [3, 4]. As biological implications, during infection of pathogens into human body, the microbes transport along tracheal, lymphangion, or even blood vessel. The transport problem is also involved in some special therapy, where engineered bacteria are transported along blood vessel to tumor and stimulate the immune system to kill the cancer cells [5]. Thus the knowledge of how active particles, such as active Brownian particles (ABPs) and run-and-tumble particles (RTPs) [6, 7] which are often used in describing the motion of microbes such as bacteria [8–11], transport along a tube can help us understand these processes.

Passive particles transported in 2D- and 3D-channels have been studied for a long time [12–19]. In the seminal work of Jacobs [12], the time evolution of 1D density of passive particles along a tube can be reduced to the Fick-Jacobs (FJ) equation, where the motion of the passive particles can be regarded as quasi-1D subjected to an effective potential. This potential is often referred to as entropy potential $V = -k_B T \log A$ [13] because it can be rewritten as $V = -TS$, where $S = k_B \log A$ is entropy given that the area A of a cross section of the tube is proportional to the probability density function ρ of finding a particle around the cross section. This concept is handy when we consider the first-passage problems of particles in tubes, and simplifies the analysis of some phenomenon such as stochastic resonance [20, 21].

It has not been fully explored, however, if the active particles moving in a long tube can be treated in the same framework. Unlike passive particles, the active particles often accumulate around the hard wall [22–24] due to their persistent motion, which leads to a decaying particle density profile from the wall into the bulk. Thus the 1D density of active particles is not proportional to the area of cross sections of a tube, and a correction accounting for the boundary accumulation which is proportional to the perimeter of the cross sections should be added. The correction will be significant if the persistence length of active particles is sufficiently large.

The cases in the limit of narrow tubes and large translational thermal noises has been discussed [4], where the width of the tube is comparable to the diameter of particles. They extended the FJ framework and found the interaction between the activity of particles and the boundaries cannot be characterized by a conservative potential, and asymmetric channels can provoke ratchet flow along the tube. But the channels of intermediate and large width are remain unexplored.

In this article, we analytically calculate the time evolution of the 1D probability density of active particles moving in long channels with hard boundaries, and show the system can be reduced to 1D particles moving in an effective entropy potential in the passive limit. The activity of particles does not only contribute to the effective temperature in the potential, but also influences the effective width of the channel sensed by the particles. Then we show how the effective entropy potential can be used in estimating the steady-state 1D density and the mean-first-passage time of a particle escaping out of a spindle channel.

Fick-Jacobs equation of passive particles.— Consider passive Brownian particles with diffusion constant D moving in a long channel with non-slip hard boundaries along the x -axis, with cross section area $A(x)$ as a function of position x . The time evolution of the multi-dimensional probability density $P(\mathbf{x})$ satisfies the diffusion equation $\frac{\partial P}{\partial t} = D\Delta P$, with non-slip boundary conditions $\mathbf{n} \cdot \nabla P = 0$, where \mathbf{n} is unit vectors normal to the boundaries.

If $A(x)$ is a slow-varying function of x , the time evolution of 1D density profile $\rho(x) = \int P(\mathbf{x}) dS$ can be described by the Fick-Jacobs equation, which can be obtained by integrating the diffusion equation along all the spatial dimensions other than x [12, 13],

$$\frac{\partial \rho}{\partial t} = \frac{\partial}{\partial x} \left(DA(x) \frac{\partial \rho}{\partial x} \frac{1}{A(x)} \right). \quad (1)$$

Eq. (1) can be interpreted as 1D Brownian particles moving in an 1D effective potential $V(x) = -D \log A(x)$. For moderate large $|A'(x)|$, the accuracy of the equation can be improved by replacing the diffusion constant by $\tilde{D}(x) = D/[1 + A'(x)^2]^\alpha$, where $\alpha = 1/3$ for 2D and $\alpha = 1/2$ for 3D [14, 16].

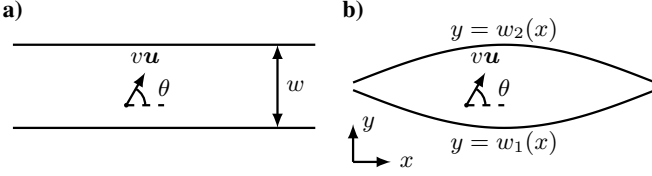


FIG. 1. **Active particles inside homogeneous (a) and corrugated tubes (b).** We impose periodic boundary condition in the x direction.

Active particles under confinement with non-slip boundary conditions.— Before investigating the FJ equation of active particles, we briefly revise the calculations of the steady-state density profile of active particles in a channel with non-slip hard and homogeneous boundaries in Ref. [24]. Some references assuming a vanishing thermal translational noise [25, 26] are beyond the scope of this article. Consider self-propelled particles with constant speed v and persistence time τ , subjected to thermal translational diffusion with constant D . The channel is translational symmetric along x -axis with width w . The boundaries locate at $y = 0$ and w (Fig. 1a).

Here we consider 2D non-interacting spherical ABPs for clarity. The calculations for RTPs are similar. The trajectory $\mathbf{r}(t)$ of a single particle can be described by the Itô-Langevin equations

$$\dot{\mathbf{r}} = v\mathbf{u}(\theta) + \sqrt{2D}\boldsymbol{\xi}(t), \quad \dot{\theta} = \sqrt{\frac{2}{\tau}}\eta(t). \quad (2)$$

$\boldsymbol{\xi}(t)$ and $\eta(t)$ are Gaussian white noises satisfying $\langle \xi_i(t)\xi_j(t') \rangle = \delta_{ij}\delta(t-t')$, $\langle \eta(t)\eta(t') \rangle = \delta(t-t')$. $\mathbf{u}(\theta) \equiv (\cos\theta, \sin\theta)$ is the orientation vector of the particle. Denoting $\rho(y) \equiv \langle \sum_i \delta(y - y_i) \rangle$ as the 1D density profile of the particles, $\mathbf{m}(y) \equiv \langle \sum_i \mathbf{u}_i \delta(y - y_i) \rangle$ as the polarization profile, and $\mathbf{Q}(y) \equiv \langle \sum_i (\mathbf{u}_i \mathbf{u}_i - \mathbf{I}/2) \delta(y - y_i) \rangle$ as the nematic tensor, we have the same dynamic equations valid for both ABPs and RTPs [6, 7]

$$\frac{\partial \rho}{\partial t} = -v\nabla \cdot \mathbf{m} + D\Delta\rho, \quad (3)$$

$$\frac{\partial \mathbf{m}}{\partial t} = -\frac{v}{2}\nabla\rho - v\nabla \cdot \mathbf{Q} - \frac{1}{\tau}\mathbf{m} + D\Delta\mathbf{m}. \quad (4)$$

The flow of particles with orientation \mathbf{u} is $\boldsymbol{\Gamma} \equiv v\mathbf{u}(\theta)\Phi(\mathbf{r}, \mathbf{u}; t) - D\nabla\Phi$, where $\Phi(\mathbf{r}, \mathbf{u}; t)$ is the probability density function of finding a particle at position \mathbf{r} with orientation \mathbf{u} . The non-slip boundary condition $\mathbf{e}_y \cdot \boldsymbol{\Gamma} = 0$ now reads $vm_y = D\rho'(y)$, $v(\rho/2 + Q_{yy}) = Dm'_y$ at $y = 0$ and w .

Considering the translational symmetry of the system along x , $m_x = 0$ and $Q_{yx} = 0$. To close the equations, we assume $\mathbf{Q} = \mathbf{0}$, and obtain the solution of the density profile

$$\rho_{\text{hm}}(y) = \rho_b \frac{D_a(e^{-y/\ell_b} + e^{(y-w)/\ell_b}) + D(1 + e^{-w/\ell_b})}{2D_a e^{-w/2\ell_b} + D(1 + e^{-w/\ell_b})}, \quad (5)$$

where $\ell_b \equiv D/\sqrt{(D_a + D)/\tau}$ is the characteristic length scale of the thickness of the boundary layer, $D_a \equiv v^2\tau/2$ is the active contribution of the effective diffusion constant, $D_{\text{eff}} \equiv D_a + D$, and ρ_b is the bulk density at $y = w/2$. Then $m_{\text{hm}}(y) \equiv m_y(y) = D\rho'(y)/v$. If $w \gg \ell_b$, we have the profile near $y = 0$ as

$$\rho_{\text{hm}}(y) \approx \rho_b \left(\frac{D_a}{D} e^{-y/\ell_b} + 1 \right). \quad (6)$$

The same result has been obtained in Ref. [24]. The number of excess particles accumulated near the boundary can be estimated by $n_{\text{db}}\rho_b \equiv \rho_b \int_0^\infty dy D_a e^{-y/\ell_b} / D = \rho_b D_a \ell_b / D$.

Hence truncating at the second order in the moment expansion of Φ , the density profile near a hard boundary is exponentially decreasing away from the wall, with a boundary layer of characteristic thickness ℓ_b . We tested the approximation in quasi-1D agent-based simulations, where we reject the motion of a particle if it moves out of the confined region. The numerical results show a slower decay than Eq. (6), which is due to a non-zero $\nabla \cdot \mathbf{Q}$. A finer estimation can be obtained by truncating at higher order in the moment expansion of Φ , where we can identify more exponential components accounting for a slower decay. For $w \gg \ell_b$ and $w \gg \ell_p$, where $\ell_p \equiv v\tau$ is the persistent length of the particle, the approximation Eq. (6) is a reasonable estimation of the density profile (Fig. 2).

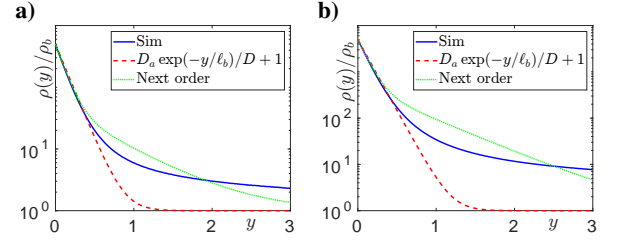


FIG. 2. **The density profile of ABPs near the homogeneous hard wall.** The wall is located at $y = 0$. The green curves are obtained by preserving a finite \mathbf{Q} and assuming the third moment can be neglected. a) $\tau = 100$. b) $\tau = 1000$. For both figures, $w = 10^4$, $v = 1$, $D = 0.1$. To calculate the density profile, the size of the bins is 0.1.

We note that under the condition of small Peclet number $\text{Pe} \equiv v/\sqrt{D/\tau}$, the expansion of Eq. (6) in v is consistent with Eq. (15) of Ref. [22], where the similar result is derived in 3D space.

Fick-Jacobs equation of active particles in 2D channels.— Now we are ready to derive a Fick-Jacobs-like equation for non-interacting ABPs. The results will be similar for RTPs. We consider a long channel in 2D with varying widths. The top and bottom boundaries of the channel are described by $y = w_1(x)$ and $y = w_2(x)$ respectively (Fig. 1b). The Fokker-Planck (FP) equation of the probability density function (PDF) $\Phi(x, y, \mathbf{u}; t)$ of 2D ABPs is

$$\frac{\partial \Phi}{\partial t} = -\nabla \cdot (v\mathbf{u}\Phi) + D\Delta\Phi + \frac{1}{\tau}\partial_{\theta\theta}\Phi. \quad (7)$$

Denoting $\tilde{\Phi}(x, \mathbf{u}) = \int_{w_1(x)}^{w_2(x)} \Phi(x, y, \mathbf{u}) dy$, we have

$$\begin{aligned} \frac{\partial \tilde{\Phi}}{\partial t} &= -v \cos \theta \frac{\partial \tilde{\Phi}}{\partial x} + D \Delta \tilde{\Phi} + \frac{1}{\tau} \partial_{\theta\theta} \tilde{\Phi} \\ &\quad - D \frac{\partial}{\partial x} [\Phi(x, w_2(x), \mathbf{u}) w_2'(x) - \Phi(x, w_1(x), \mathbf{u}) w_1'(x)]. \end{aligned} \quad (8)$$

If $|w_i'(x)| \ll 1$, as a zeroth order approximation, $\Phi(x, w_1(x), \mathbf{u}) = \Phi(x, w_2(x), \mathbf{u}) \approx \Phi^{\text{bd}}$, where Φ^{bd} is the boundary value of Φ calculated in a homogeneous channel. Denoting $w(x) = w_2(x) - w_1(x)$, we have

$$\frac{\partial \tilde{\Phi}}{\partial t} = -v \cos \theta \frac{\partial \tilde{\Phi}}{\partial x} + D \Delta \tilde{\Phi} + \frac{1}{\tau} \partial_{\theta\theta} \tilde{\Phi} - D \frac{\partial}{\partial x} [\Phi^{\text{bd}} w'(x)]. \quad (9)$$

Eq. (9) resembles the form of FJ equation if we can relate the boundary value Φ^{bd} with the integrated PDF $\tilde{\Phi}$, but it's difficult due to the lack of an analytic solution of the FP equation in a homogeneous channel with non-slip boundary conditions. Again we calculate the moment expansion of $\tilde{\Phi}$. Defining 1D integrated density $\tilde{\rho} \equiv \int \tilde{\Phi} d\theta$, first moment $\tilde{m}_1 \equiv \int \tilde{\Phi} \cos \theta d\theta$, and second moment $\tilde{m}_2 \equiv \int \tilde{\Phi} \cos^2 \theta d\theta$, we have

$$\begin{aligned} \frac{\partial \tilde{\rho}}{\partial t} &= -v \frac{\partial \tilde{m}_1}{\partial x} + D \frac{\partial^2 \tilde{\rho}}{\partial x^2} - D \frac{\partial}{\partial x} [\rho^{\text{bd}} w'(x)], \quad (10) \\ \frac{\partial \tilde{m}_1}{\partial t} &= -\frac{v}{2} \frac{\partial (\tilde{\rho} + \tilde{m}_2)}{\partial x} - \frac{\tilde{m}_1}{\tau} + D \frac{\partial^2 \tilde{m}_1}{\partial x^2} - D \frac{\partial [m_1^{\text{bd}} w'(x)]}{\partial x}. \end{aligned} \quad (11)$$

The key assumption towards a FJ equation is that the length of tube $L \gg w(x)$ such that the local equilibrium is reached in the y -direction at any x . Similarly we assume steady states in the y -direction. Keeping only the terms of order $w'(x)$, the shifted density $\rho(x, y)$ in the y direction can be approximated by Eq. (5), with $w = w(x)$ and replacing y by $y - w_2(x)$. $\tilde{\rho} = \int_{w_1}^{w_2} \rho(x, y) dy$ gives the relation between $\tilde{\rho}$ and ρ^{bd}

$$\rho^{\text{bd}} = \frac{D_{\text{eff}}}{Dw(x) + 2D_a \ell_b \tanh(w(x)/2\ell_b)} \tilde{\rho}, \quad (12)$$

If $v \rightarrow 0$, $\rho^{\text{bd}} \rightarrow \tilde{\rho}/w(x)$ which gives the FJ equation for passive particles. From Eq. (12), the density field is equivalent to be subjected to an effective potential

$$V(x) = -D \int^x \frac{D_{\text{eff}} w'(x)}{Dw(x) + 2D_a \ell_b \tanh(w(x)/2\ell_b)} dx. \quad (13)$$

The expression of $V(x)$ can be simplified if we consider the wide channel limit $w(x) \gg \ell_b$. Then $\tanh(w(x)/2\ell_b) \approx 1$, and the effective entropy potential is

$$V(x) = -D_{\text{eff}} \log \left[\frac{2D_a \ell_b}{D} + w(x) \right]. \quad (14)$$

Unfortunately, m_1^{bd} cannot be related to \tilde{m}_1 in the same form as Eq. (12) in the zeroth order approximation, because

$m_1 = 0$ in homogeneous channels. Thus in the zeroth order approximation, the activity of the particles only modifies the effective diffusion constant $D_{\text{eff}} \equiv D + v^2 \tau / 2$ and the effective potential Eq. (14), while the dynamics of the 1D density is passive if we consider \tilde{m}_1 relax much faster than $\tilde{\rho}$, and if $\tilde{\rho}$ is smooth such that the higher order derivatives can be neglected.

$$\frac{\partial \tilde{\rho}}{\partial t} = D_{\text{eff}} \frac{\partial^2 \tilde{\rho}}{\partial x^2} + \frac{\partial}{\partial x} [\tilde{\rho} V'(x)]. \quad (15)$$

The effective potential Eq. (14), however, is not obtained by replacing the diffusion constant D in the passive entropy potential $V = -D \log w$ by D_{eff} , due to the accumulation of particles near boundaries. The boundary layer smooths the varying width of the channel by adding a constant $2n_{\text{bd}} = 2D_a \ell_b / D$ proportional to the number of excess particles accumulated near the two boundaries. We note $\ell_b \sim D_a^{-1/2}$ at sufficiently large D_a , and $n_{\text{bd}} \sim D_a^{1/2}$. At large D_a , a thin boundary layer can contribute significantly in the total density. The particles then spend most of the time near the boundary, and do not feel the change in the width of the channel.

We can bring back the \tilde{m}_1 field by taking the slope of boundaries into account. In the limit of wide channels, we can assume local translational symmetry along the tangential direction of the boundaries. Then at the boundary, \mathbf{m} is locally normal to the boundary, and m_1^{bd} is \mathbf{m} projected on the x -axis. $m_1^{\text{bd}} = m_{\text{hm}}(0) \sin \arctan[w'(x)/2] \approx m_{\text{hm}}(0) w'(x)/2$. In the bulk $\mathbf{m} = 0$, and only the two non-zero boundary layers contribute to \tilde{m}_1 . $\tilde{m}_1 = 2 \int_0^\infty dy m_{\text{hm}}(y) w'(x)/2$. From Eq. (6), $m_1^{\text{bd}} = \tilde{m}_1 / 2\ell_b$. Thus the polarization field is equivalent to be subjected to another effective potential

$$V_m(x) = -\frac{D}{2\ell_b} \log w(x). \quad (16)$$

Then we have the FJ equation for the ABPs under the first order approximation of $w'(x)$,

$$\begin{aligned} \frac{\partial \tilde{\rho}}{\partial t} &= -v \frac{\partial \tilde{m}_1}{\partial x} + D \frac{\partial^2 \tilde{\rho}}{\partial x^2} + \frac{\partial}{\partial x} [\tilde{\rho} V'(x)], \quad (17) \\ \frac{\partial \tilde{m}_1}{\partial t} &= -\frac{v}{2} \frac{\partial (\tilde{\rho} + \tilde{m}_2)}{\partial x} - \frac{\tilde{m}_1}{\tau} + D \frac{\partial^2 \tilde{m}_1}{\partial x^2} + \frac{\partial}{\partial x} [\tilde{m}_1 V_m'(x)]. \end{aligned} \quad (18)$$

The activity of the particles is partially restored. But since $V_m(x) \neq V(x)$, the 1D dynamics of 2D ABPs can not be described using a single conservative potential.

1D steady-state density profile of ABPs along 2D corrugated channels.— Now we consider the 1D steady-state density of ABPs in long channels with slow varying width. If the second moment \tilde{m}_2 is neglectable, and the density profile is smooth enough such that all the terms of order $o(\partial_x^2 \tilde{\rho})$ can be neglected, we have the steady state distribution of $\tilde{\rho}$ as

$$\tilde{\rho}(x) \propto \exp \left(- \int^x \frac{V'(x)}{D_{\text{eff}} + D_a \tau V_m''(x)} dx \right). \quad (19)$$

If $|V_m''(x)| \ll 1/(D_a\tau)$, not surprisingly, the 1D steady-state distributions inside slow-varying channels have the form of Boltzmann weights with the effective temperature D_{eff} , $\tilde{\rho}(x) \propto \exp(-V(x)/D_{\text{eff}}) = 2n_{\text{bd}} + w(x)$, since at large scales ABPs resemble passive Brownian particles. The effective entropy potential, however, should be corrected by the active accumulation of the particles.

The calculations can be verified by agent-based simulations (Fig. 3a-b). It clearly shows the 1D density profile is flattened due to the existence of boundary layers. Because the number of particles absorbed by the boundaries is independent of the width of the boundary, the contribution to the density profile from the accumulated particles smooths out the effective potential and thus the density profile. We note that the approximation does not hold if A/L is large such that $|w'(x)|$ is not small.

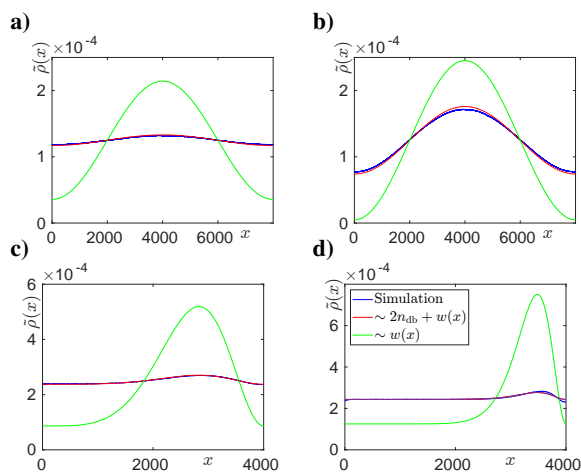


FIG. 3. The 1D density profile of ABPs along a corrugated 2D channel. The boundary is located at $y = w_{1,2}(x) = \pm[A(1 - \cos(2\pi x/L))/2 + C_0]$ with $A = 50$ (a) and 500 (b), or $y = w_{1,2} = \pm[A(1 - \cos(2\pi(x/L)^N))/2 + C_0]$ with $N = 2$ (c) and $N = 5$ (d), $A = 50$. The theoretical estimation of the density profile is obtained by $\exp(-V(x)/D_{\text{eff}})$. The red lines are calculated using the $V(x)$ in Eq. (14), while the green lines are using the passive counterpart $V(x) = -D_{\text{eff}} \log w(x)$. For both figures, $L = 8 \times 10^3$ for symmetric channels and $L = 4 \times 10^3$ for asymmetric ones, $C_0 = 10$, $v = 5$, $\tau = 100$, $D = 0.1$. To calculate the density profile, the size of the bins is 1.

The Boltzmann weights can be tested in asymmetric channels as well (Fig. 3c-d). We find that if the boundary varies too fast, the approximation assuming small $|w'(x)|$ can not give precise estimations. We note that in principle these asymmetric channels should provoke non-equilibrium ratchet flows, which cannot be estimated by equilibrium Boltzmann weights. It is possible to predict a weak ratchet flow from Eq. (19), but the ratchet flow in long channels with slow varying width is weak, and thus the estimation is difficult to check numerically.

Generalization to 3D tubes.— We can generalize the idea of the effective potential to 3D tubes, along the x direction without loss of generality. But we note that the difference in

curvature of the boundary in the yz plane can also induce particle accumulations at large curvature, and the full solution can thus be highly non-trivial [27]. If the radius of the boundaries of cross sections is much larger than ℓ_p such that the density profile near the boundary can be approximated by that near a homogeneous flat boundary, we can approximate the integration of the density profile in a cross section in the yz plane as the sum of contributions from the bulk and the boundary layer. We have $\tilde{\rho}(x) \approx \rho_b[A(x) + n_{\text{bd}}P(x)]$, where $A(x)$ is the area of the cross section of the tube along the yz plane at x , and $P(x)$ is the perimeter of the cross section. Thus we have

$$V(x) = -D_{\text{eff}} \log [n_{\text{bd}}P(x) + A(x)]. \quad (20)$$

Note that $n_{\text{bd}} = D_a\ell_b/D$ where $D_a = v^2\tau/d$ in d -dimensional space. If the cross section of the tube at any position x is circular with radius $R(x)$, $P(x) = 2\pi R(x)$ and $A(x) = \pi R(x)^2$, we have $V(x) = -D_{\text{eff}} \log [2n_{\text{bd}}R(x) + R(x)^2]$.

We tested the estimation with the simulations of RTPs in 3D tube with rotational symmetry along the x axis (Fig. 4b). We note that the estimation is valid only for sufficiently large C_0 to ensure the curvature of the tube is neglectable. Otherwise the accumulation of particles around large curvature will further flatten the density profile (Fig. 4a). The agreement also indicates the estimation from ABPs applies to RTPs directly because they share the same dynamics Eq. (3)-(4) of ρ and \mathbf{m} .

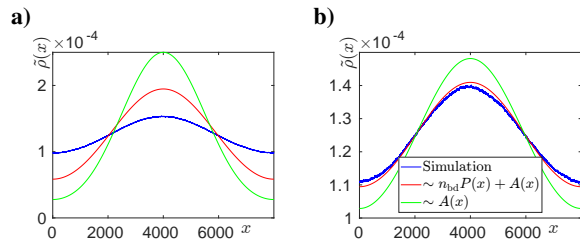


FIG. 4. The 1D density profile of RTPs along a corrugated 3D tube. The cross sections in yz plane is always circular, with radius $R(x) = R_0[1 - \cos(2\pi x/L)]/2 + C_0$ and $C_0 = 50$ (a) and 500 (b). The theoretical estimation of the density profile is obtained by $\exp(-V(x)/D_{\text{eff}})$. The red lines are calculated using the $V(x)$ in Eq. (20), while the green lines are using the passive counterpart $V(x) = -2D_{\text{eff}} \log R(x)$. For both figures, $L = 8 \times 10^3$, $R_0 = 100$, $v = 5$, $\tau = 100$, $D = 0.1$. To calculate the density profile, the size of the bins is 1.

Mean escape time of an active particle from a spindle chamber.— With the generalized entropy potential (14), one can calculate the mean first passage time of one particle escaping from a spindle chamber as shown in Fig. 1b. If $|V_m''(x)| \ll 1$, the mean first passage time t_{MFP} of a particle starting from the middle of the spindle $x = L/2$ with random orientation and reaching one of the necks at $x = 0$ or L is given by Kramer's seminal work [28]

$$t_{\text{MFP}} \sim \frac{\pi}{2\sqrt{|V''(L/2)V''(0)|}} \exp\left(\frac{V(0) - V(L/2)}{D_{\text{eff}}}\right). \quad (21)$$

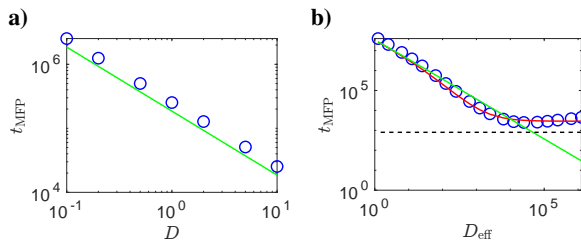


FIG. 5. **The mean first passage time of a passive particle (a) or an ABP (b) moving from the middle of a spindle ($x = L/2$) to one of the necks ($x = 0$ or L).** The width of the spindle is defined as $w(x) = A[1 - \cos(2\pi x/L)] + 2C_0$. $L = 8000$, $C_0 = 10$, $A = 100$ (a) or 500 (b). The simulation data are shown by the circles. The red lines are estimated from the effective potential given by Eq. (14), while the green lines are from Eq. (21) with $V = -D_{\text{eff}} \log w(x)$. The black dashed lines indicate the running time $L/(2v)$ for a particle from $x = L/2$ to one of the necks. $v = 5$ and $D = 0.1$ for the ABPs, and τ ranges from 10^{-1} to 10^5 .

We note a factor of $1/4$ because the particles can escape from two sides, and we only calculate the time ending at the peak of the entropy potential when particles have probability $1/2$ to escape. For passive particles, $V = -D \log w(x)$. Assuming the width of the chamber is $w(x) = A[1 - \cos(2\pi x/L)] + 2C_0$, we have $t_{\text{MFPP}} \sim (A + C_0)^{3/2} L^2 / (4\pi A \sqrt{C_0} D) \propto 1/D$.

The $1/D$ scaling of passive particles can be checked from simulations, as shown in Fig. 5a. t_{MFPP} for active particles, however, does not satisfy the $1/D_{\text{eff}}$ scaling because the activity does not only contribute to the effective diffusion constant, but also to the effective width of the channel. As shown in Fig. 5b, the MFPT first decreases with D_{eff} similar as passive particles, and then starts to increase at an optimal D_{eff} . Unlike passive particles, ABPs have finite moving speed, and the time for ABPs to travel $L/2$ is bounded by $L/(2v)$. For larger D_{eff} , the time for ABPs to be stuck near the boundary increases with the activity of the particles, and thus increases the time for ABPs to escape from the channel.

We note that Eq. (21) with the effective potential Eq. (14) (red lines in Fig. 5b) describe qualitatively the transition away from the passive regime. But at large τ the condition that $w \gg \ell_p$ cannot be held and Eq. (14) fails. Thus we cannot expect quantitative agreement at large D_{eff} .

Discussion.— In this article we extended the Fick-Jacobs equation from passive particles to active particles in the limit of a wide and long tube with slow varying width. We show that the generalized entropy potential can better predict the steady-state 1D density profile along the tube than simply replacing the diffusion constant by its effective counterpart, and give qualitatively the mean first passage time from Kramers' law. We use ABPs in the analysis, but all the calculations holds automatically for RTPs, because ABPs and RTPs share the same dynamics of the first two moments in the moment expansion of the probability density functions [6, 7] which is used in the analysis. We note that the calculations require a finite D , which leads to a continuous density profile near the

boundary and non-zero ℓ_b .

We have so far assumed $|w'(x)| \ll 1$ and the curvature of the boundary can be neglected. The estimation relies on a wide tube approximation $w(x) \gg \ell_b$, such that contribution from the boundary layers and the bulk can be separated. How the calculations can be corrected considering the deviation from local steady state in the y -direction at finite $w'(x)$ remains a challenging question. And for a finite $w(x)$, it is difficult to approximate m_1^{bd} because there is no local symmetry can be applied. For a thin tube it has been shown that the dynamics cannot be characterized by a conservative potential [4]. Another limitation of the work is that we assume the nematic tensor \mathbf{Q} to be vanishing, which require w to be sufficiently large compared with persistence length ℓ_p . The higher order moments which are important for the density profile remain out of reach.

In this work we considered spherical particles. Elongated active particles can accumulate near the boundary as well [29]. Because elongated particles align with boundaries, the probability of leaving the boundary decreases with larger aspect ratio, and the number of accumulated particles increases with the length of the particle in the dilute limit [29]. We can expect larger boundary effect with elongated particles.

So far we considered non-interacting particles. For dense particles the interactions will reshape the density profiles near the wall. Particles with repulsive interactions still accumulate near the wall, but the width of the boundary layer will be larger than non-interacting particles while the number of accumulated particles will be smaller because of volume exclusion.

The possible relevant experimental setup can be colloid particles driven by an external magnetic field moving in PDMS microfluid channels, if the contribution from hydrodynamics of the water can be neglected and the boundaries can be considered hard walls. Robots moving in a track with varying width could be a cleaner experimental system.

The author thanks Xiaqing Shi, Hepeng Zhang, Hugues Chaté, and Masaki Sano for helpful discussions and critical comments. The author acknowledges support from the start-up grant NH10800621 from Soochow University.

* yfzhao2021@suda.edu.cn

- [1] J. chun Wu, Q. Chen, and B. quan Ai, Entropic transport of active particles driven by a transverse ac force, *Physics Letters A* **379**, 3025 (2015).
- [2] L. Caprini, F. Cecconi, and U. Marini Bettolo Marconi, Transport of active particles in an open-wedge channel, *The Journal of Chemical Physics* **150**, 144903 (2019), <https://doi.org/10.1063/1.5090104>.
- [3] B.-Q. Ai, Y.-F. He, and W.-R. Zhong, Entropic ratchet transport of interacting active brownian particles, *The Journal of Chemical Physics* **141**, 194111 (2014), <https://doi.org/10.1063/1.4901896>.
- [4] P. Magaretti and H. Stark, Model microswimmers in channels

- with varying cross section, *The Journal of Chemical Physics* **146**, 174901 (2017), <https://doi.org/10.1063/1.4981886>.
- [5] L. Shi, B. Yu, C.-H. Cai, W. Huang, B.-J. Zheng, D. K. Smith, and J.-D. Huang, Combined prokaryotic–eukaryotic delivery and expression of therapeutic factors through a primed autocatalytic positive-feedback loop, *Journal of Controlled Release* **222**, 130 (2016).
- [6] M. E. Cates and J. Tailleur, When are active Brownian particles and run-and-tumble particles equivalent? Consequences for motility-induced phase separation, *Europhys. Lett.* **101**, 20010 (2013).
- [7] A. P. Solon, M. E. Cates, and J. Tailleur, Active brownian particles and run-and-tumble particles: A comparative study, *The European Physical Journal Special Topics* **224**, 1231 (2015).
- [8] H. C. Berg and D. A. Brown, Chemotaxis in *Escherichia coli* analysed by three-dimensional tracking, *Nature* **239**, 500 (1972).
- [9] L. G. Wilson, V. A. Martinez, J. Schwarz-Linek, J. Tailleur, G. Bryant, P. N. Pusey, and W. C. K. Poon, Differential dynamic microscopy of bacterial motility, *Phys. Rev. Lett.* **106**, 018101 (2011).
- [10] V. A. Martinez, R. Besseling, O. A. Croze, J. Tailleur, M. Reufer, J. Schwarz-Linek, L. G. Wilson, M. A. Bees, and W. C. K. Poon, Differential dynamic microscopy: A high-throughput method for characterizing the motility of microorganisms, *Biophys. J.* **103**, 1637 (2012).
- [11] A. Curatolo, N. Zhou, Y. Zhao, C. Liu, A. Daerr, J. Tailleur, and J. Huang, Cooperative pattern formation in multi-component bacterial systems through reciprocal motility regulation, *Nat. Phys.*, 1 (2020).
- [12] M. H. Jacobs, *Diffusion Process* (Springer-Verlag, 1967).
- [13] R. Zwanzig, Diffusion past an entropy barrier, *The Journal of Physical Chemistry* **96**, 3926 (1992).
- [14] D. Reguera and J. M. Rubí, Kinetic equations for diffusion in the presence of entropic barriers, *Phys. Rev. E* **64**, 061106 (2001).
- [15] D. Reguera, G. Schmid, P. S. Burada, J. M. Rubí, P. Reimann, and P. Hänggi, Entropic transport: Kinetics, scaling, and control mechanisms, *Phys. Rev. Lett.* **96**, 130603 (2006).
- [16] P. S. Burada, G. Schmid, D. Reguera, J. M. Rubí, and P. Hänggi, Biased diffusion in confined media: Test of the fick-jacobs approximation and validity criteria, *Phys. Rev. E* **75**, 051111 (2007).
- [17] X. Yang, C. Liu, Y. Li, F. Marchesoni, P. Hänggi, and H. P. Zhang, Hydrodynamic and entropic effects on colloidal diffusion in corrugated channels, *Proceedings of the National Academy of Sciences* **114**, 9564 (2017), <https://www.pnas.org/content/114/36/9564.full.pdf>.
- [18] S. Marbach, D. S. Dean, and L. Bocquet, Transport and dispersion across wiggling nanopores, *Nature Physics* **14**, 1108 (2018).
- [19] X. Yang, Q. Zhu, C. Liu, W. Wang, Y. Li, F. Marchesoni, P. Hänggi, and H. P. Zhang, Diffusion of colloidal rods in corrugated channels, *Phys. Rev. E* **99**, 020601 (2019).
- [20] P. S. Burada, G. Schmid, D. Reguera, M. H. Vainstein, J. M. Rubi, and P. Hänggi, Entropic stochastic resonance, *Phys. Rev. Lett.* **101**, 130602 (2008).
- [21] P. K. Ghosh, F. Marchesoni, S. E. Savel'ev, and F. Nori, Geometric stochastic resonance, *Phys. Rev. Lett.* **104**, 020601 (2010).
- [22] J. Elgeti and G. Gompper, Wall accumulation of self-propelled spheres, *EPL (Europhysics Letters)* **101**, 48003 (2013).
- [23] A. P. Solon, Y. Fily, A. Baskaran, M. E. Cates, Y. Kafri, M. Kardar, and J. Tailleur, Pressure is not a state function for generic active fluids, *Nature Physics* **11**, 673 (2015).
- [24] A. Duzgun and J. V. Selinger, Active brownian particles near straight or curved walls: Pressure and boundary layers, *Phys. Rev. E* **97**, 032606 (2018).
- [25] L. Angelani, Confined run-and-tumble swimmers in one dimension, *Journal of Physics A: Mathematical and Theoretical* **50**, 325601 (2017).
- [26] C. G. Wagner, M. F. Hagan, and A. Baskaran, Steady states of active brownian particles interacting with boundaries (2021), [arXiv:2109.06353 \[cond-mat.soft\]](https://arxiv.org/abs/2109.06353).
- [27] N. Nikola, A. P. Solon, Y. Kafri, M. Kardar, J. Tailleur, and R. Voituriez, Active particles with soft and curved walls: Equation of state, ratchets, and instabilities, *Phys. Rev. Lett.* **117**, 098001 (2016).
- [28] H. Kramers, Brownian motion in a field of force and the diffusion model of chemical reactions, *Physica* **7**, 284 (1940).
- [29] J. Elgeti and G. Gompper, Self-propelled rods near surfaces, *EPL (Europhysics Letters)* **85**, 38002 (2009).